

## A Case Study of Interstellar Material Delivery: $\alpha$ Centauri

COLE R. GREGG <sup>1,2</sup> AND PAUL A. WIEGERT <sup>1,2</sup>

<sup>1</sup>*Department of Physics and Astronomy  
The University of Western Ontario  
London, Canada*

<sup>2</sup>*Institute for Earth and Space Exploration (IESX)  
The University of Western Ontario  
London, Canada*

(Received December 17, 2024; Revised Jan 24, 2025; Accepted January 31, 2025)

### ABSTRACT

Interstellar material has been discovered in our Solar System, yet its origins and details of its transport are unknown. Here we present  $\alpha$  Centauri as a case study of the delivery of interstellar material to our Solar System.  $\alpha$  Centauri is a mature triple star system that likely harbours planets, and is moving towards us with the point of closest approach approximately 28,000 years in the future. Assuming a current ejection model for the system, we find that such material can reach our Solar System and may currently be present here. The material that does reach us is mostly a product of low ( $< 2 \text{ km s}^{-1}$ ) ejection velocities, and the rate at which it enters our Solar System is expected to peak around the time of  $\alpha$  Centauri's closest approach. If  $\alpha$  Centauri ejects material at a rate comparable to our own Solar System, we estimate the current number of  $\alpha$  Centauri particles larger than 100 m in diameter within our Oort Cloud to be  $10^6$ , and during  $\alpha$  Centauri's closest approach, this will increase by an order of magnitude. However, the observable fraction of such objects remains low as there is only a probability of  $10^{-6}$  that one of them is within 10 au of the Sun. A small number ( $\sim 10$ ) meteors  $> 100 \mu\text{m}$  from  $\alpha$  Centauri may currently be entering Earth's atmosphere every year: this number is very sensitive to the assumed ejected mass distribution, but the flux is expected to increase as  $\alpha$  Centauri approaches.

*Keywords:* Interstellar Objects(52) — Meteor Radiants(1033) — Meteor Streams(1035)

### 1. INTRODUCTION

To date, there have been two discoveries of macroscopic objects from outside our Solar System: 1I/'Oumuamua (Meech et al. 2017) and 2I/Borisov (Guzik et al. 2020). At smaller sizes, in situ dust detectors on spacecraft (Grün et al. 1997; Baguhl et al. 1995; Altobelli et al. 2003) have also unambiguously detected interstellar particles. At intermediate sizes, the claims of interstellar meteors detected remain controversial. This is because usually the only indicator of the interstellar nature of a particle is its hyperbolic excess velocity, which is very sensitive to measurement error (Hajdukova et al. 2020; Hajduková et al. 2024).

In any case, the details of the travel of interstellar material as well as its original sources remain unknown. Understanding the transfer of interstellar material carries significant implications as such material could seed the formation of planets in newly forming planetary systems (Grishin et al. 2019; Moro-Martín & Norman 2022), while serving as a medium for the exchange of chemical elements, organic molecules, and potentially life's precursors between star systems - panspermia (Grishin et al. 2019; Adams & Napier 2022; Osmanov 2024; Smith & Sinapayen 2024).

Here we aim to increase our understanding of interstellar transport by performing a case study of one particular nearby star system,  $\alpha$  Centauri ( $\alpha$  Cen), and focusing on transfer within the near term (last 100 Myr). The fundamental questions guiding this study are: Can  $\alpha$  Cen plausibly be ejecting material at the current time, and if so, would we expect this material to arrive at our Solar System? What would be the expected characteristics of this material, including arrival direction, velocity, and flux?

The first question is whether  $\alpha$  Cen can reasonably be expected to be ejecting material at the current time. As the system is mature, we would expect much of its original protoplanetary disk to have dissipated, with some of the mass possibly retained in asteroid/Kuiper belts, or an Oort cloud (OC). Our simulations examine the relatively recent past (astronomically speaking,  $\sim 100$  Myr), well after any planet-forming phase and the disassociation of the birth cluster  $\alpha$  Cen formed in (typical lifetimes are  $\lesssim 100s$  Myr (Adams 2010)). Therefore, the primary ejection mechanisms of interest are gravitational scattering of leftover planetesimals by the stars and/or planets within the system, as well as the loss of distant OC members to galactic tidal stripping. Work much along these lines was performed by Portegies Zwart (2021), who modeled the evolution of OCs around the 200 nearest *Gaia* stars for 1 Gyr in the past to determine the density of interstellar objects (ISO) around the Sun, though  $\alpha$  Cen is not discussed in detail in that work. Here we seek to extract the specific details of the material delivery from that system near the present time, though we do not model the process of ejection in detail, but rather adopt a suitable ejection velocity distribution for the system.

Assuming that  $\alpha$  Cen is currently ejecting material, we find that such material can reach our Solar System and may currently be present here. This system is a good choice for this kind of case study for several reasons:

- It is the closest star to our Solar System, at 1.34 pc (Akeson et al. 2021). Its proximity increases the likelihood that material from this system can reach us.
- It is approaching our Solar System at  $22 \text{ km s}^{-1}$  (Evans 1967; Kervella et al. 2017; Wenger et al. 2000) and will pass within 200,000 au of the Sun in 28,000 years. Thus we can expect that the amount of material delivered to us is increasing as the effective cross-section of the Solar System increases (see Section 3 for more details).
- This is a mature (5 Gyr age (Akeson et al. 2021; Joyce & Chaboyer 2018; Thévenin et al. 2002)) triple star system that likely harbours planets. Though mature star systems likely eject less material than those in their planet-forming years, the presence of multiple stars and planets increases the likelihood of gravitational scattering of members from any remnant planetesimal reservoirs, much as asteroid or comets are currently being ejected from our Solar System.
- Two of the stars,  $\alpha$  Cen A and B, are Sun-like stars (see below for details). Their larger than typical stellar mass suggests that they likely formed from a more massive than typical protoplanetary disk, which might allow more mass to remain in unaccumulated form. In particular, the system might have developed an OC, which results from gravitational scattering of planetesimals from Neptune mass planets (Safronov 1972; Duncan et al. 1987; Tremaine 1993) which would provide a source of macroscopic bodies to eject via mechanisms much like those seen in our Solar System today (see Section 4.2).

Though we will not model the ejection process from  $\alpha$  Cen in detail here, for dynamical context we note that the system contains a  $1.1 M_{\odot}$  and  $0.9 M_{\odot}$  binary ( $\alpha$  Cen A and B, respectively: spectral types G2V, KV1 (Morel et al. 2000)) which has a highly eccentric orbit with a semi-major axis of 23.3 au and an orbital period of 80 yr (Cuello & Sucerquia 2024). The third star in the system, and the closest stellar neighbour to the Sun, is Proxima Centauri, a red dwarf orbiting the pair around 8200 au ( $0.12 M_{\odot}$ ; M5.5V) (Kervella et al. 2017; Ribas et al. 2017)). In 2016, Anglada-Escudé et al. (2016) reported the discovery of an Earth-sized planet in the habitable zone around Proxima. There have been other reports of planets in the Proxima system, including a possible sub-Earth-sized inner planet and a super-Earth or mini-Neptune (Damasso et al. 2020; Faria et al. 2022; Gratton et al. 2020). The binary system also has reported planetary candidates, but none confirmed (Rajpaul et al. 2015), although a planetary system is still believed possible (Wagner et al. 2021).

The triple star system orbits the Milky Way and is currently approaching the Sun, with an expected closest approach in  $\sim 28,000$  yr. Thus, any material currently leaving that system at low speed would be heading more-or-less towards the Solar System. Broadly speaking, if material is ejected at speeds relative to its source that are much lower than its source system's galactic orbital speed, the material follows a galactic orbit much like that of its parent, but disperses along that path due to the effects of orbital shear (Dehnen & Hasanuddin 2018; Torres et al. 2019; Portegies Zwart 2021). This behaviour is analogous to the formation of cometary meteoroid streams within our Solar System, and which can produce meteor showers at the Earth.

Next, in Section 2 we outline the methods used for this study; in Section 3 we discuss the results; then we turn to Discussion and Conclusions in Sections 4 and 5.

## 2. METHODS

The study performs the numerical integration of particles released from  $\alpha$  Centauri over the last 100 Myr to examine the fastest dynamical pathways from that system to our Solar System. The simulations are performed under the conditions described in the following sections.

### 2.1. Galactic Model

This work adopts a simple Galactic model for the Milky Way which includes only the overall time-independent gravitational field. We neglect some known perturbations that affect small particles in particular, such as ISM drag and magnetic forces. As a result, our model is only applicable to particles above a certain size, which will be addressed in more detail later in this section and in the Discussion (Section 4.1).

Our simulations are conducted in a galactocentric reference frame, with the Galactic Center (GC) positioned at the origin. A right-handed coordinate system has its x-axis extending through the Sun's projected position on the Galactic midplane towards the GC. The z-axis points towards the North Galactic Pole (NGP). The y-axis is perpendicular to the xz-plane, with its positive direction determined by the right-hand rule.

The Galactic potential model we adopt is of Miyamoto & Nagai (1975), a three-component, time-independent, axisymmetric potential. The potential is smooth and the force of gravity between individual stars is neglected. Individual star potentials can be neglected because the relaxation time,  $t_{relax}$  - the time for a body's orbit around the galaxy to be significantly perturbed by interactions with individual stars - is known to be very long in the Milky Way,  $t_{relax} \sim 10^7$  Gyr (Binney & Tremaine 2008). Significantly longer than the age of the Galaxy, indicating that the effect can be neglected over the  $\sim 100$  Myr time scales considered here.

The Galactic gravitational potential is represented by the sum of the three Galactic components:

$$\Phi = \Phi_b + \Phi_d + \Phi_h. \quad (1)$$

Provided in the galactocentric cartesian coordinate system:

$$\Phi_{b,h} = -\frac{GM_{b,h}}{\sqrt{x^2 + y^2 + z^2 + b_{b,h}^2}}, \quad (2)$$

$$\Phi_d = -\frac{GM_d}{\sqrt{x^2 + y^2 + (a_d + \sqrt{z^2 + b_d^2})}}. \quad (3)$$

In these equations,  $G$  is the universal gravitational constant,  $M_i$  is the total mass of the Galactic component, and  $a_i, b_i$  are the scale lengths reflecting the geometries of the component. The bulge and halo are portrayed as spherically symmetric, therefore only one scale length is required ( $b_{b,h}$ ). The disk is represented as a flattened spheroid, which requires two scale lengths ( $a_d$  and  $b_d$ ). The values we used to initialize our simulation are summarized in Table 1.

#### 2.1.1. Particle sizes

Murray et al. (2004) provide a detailed discussion of the influence of galactic magnetic fields, interstellar medium (ISM) drag, and grain destruction on interstellar particles, and all of these effects become increasingly important as the particle size decreases. The applicability of our model to smaller particles depends on the time and distance traveled in the ISM. We estimate that our model reliably describes rapid delivery (occurring over a fraction of a galactic rotation) for particles 100 microns and larger. A notable size-independent effect not included here is the influence of giant molecular clouds (GMC), which can accelerate the dispersion of galactic meteoroid streams. We will examine these effects post-simulation in the discussion (Section 4.1).

### 2.2. Simulation

Our simulations are based on the Runge-Kutta-Fehlberg method (Fehlberg 1974), a fourth-order integrator with variable time step, with an adopted error tolerance of  $10^{-6}$ . The barycenter of  $\alpha$  Cen is initialized into the simulation, as well as a particle representing our Sun (Table 1).

**Table 1.** The adopted values used to initialize our simulation, including the ICRS coordinates of  $\alpha$  Centauri taken from SIMBAD.

Parameter		Units	Value	References			
$M_i, i = d, b, h$		$10^{10} M_\odot$	7.91, 1.40, 69.80	[3]			
$a_i, i = d, b, h$		pc	3500, 0, 0	[3]			
$b_i, i = d, b, h$		pc	250, 350, 24000	[3]			
$r_\odot$		kpc	$8.33 \pm 0.35$	[4]			
$z_\odot$		pc	$27 \pm 4$	[2]			
$v_\odot (U, V, W)$		$\text{km s}^{-1}$	$(11.1^{+0.69}_{-0.75}, 12.24^{+0.47}_{-0.47}, 7.25^{+0.37}_{-0.36})$	[6]			
$v_{\odot, \text{circ}}$		$\text{km s}^{-1}$	$218 \pm 6$	[1]			
Galactic Centre Equatorial Coordinates ( $\alpha, \delta$ )		(hr:min:s, deg/'/'")	(17:45:37.224, -28:56:10.23)	[5]			
$\alpha$ Centauri							
Star System	$\alpha$	$\mu_\alpha$	$\delta$	$\mu_\delta$	Parallax	$v_r$	References
	(deg)	(mas yr $^{-1}$ )	(deg)	(mas yr $^{-1}$ )	(mas)	(km s $^{-1}$ )	
* alf Cen	219.873833	-3608	-60.83222194	686	742	-22.3	[7]

**References**— [1] Bovy (2015); [2] Chen et al. (2001); [3] Dauphole & Colin (1995); [4] Gillessen et al. (2009); [5] Reid & Brunthaler (2004); [6] Schönrich et al. (2010); [7] Wenger et al. (2000)

We first simulate  $\alpha$  Cen and the Sun backward from  $t = 0$  (the current epoch) a total of 100 Myr, slightly less than half of their galactic periods. From their positions and velocities at  $t \approx -100$  Myr, we allow the systems to progress forward 110 Myr, ending  $t \approx 10$  Myr in the future, with a time step of  $\sim 5000$  yr. As we propagate the systems forward again, their positions return to within the tolerance threshold at  $t = 0$ , the largest deviation observed being  $7 \times 10^{-5}$  au. As simulation time progresses, an additional 10,000 particles representing ejected material from  $\alpha$  Cen are added every 1 Myr. These particles play the role of both macroscopic telescopically observable km-class bodies such as asteroids and comets, as well as smaller (sub-mm to m) sized particles that could be detected as meteors in the Earth’s atmosphere.

### 2.2.1. Ejection model

Here we will assume that the particles ejected from  $\alpha$  Cen leave the system with some excess velocity, but we will not model their ejection in detail. Instead, we adopt a velocity distribution representative of the ejection process plausibly at work in  $\alpha$  Cen at the present time. Particles could be released by the gravitationally-driven ejection of residual planetesimals by the multiple stars in the system (Bailer-Jones et al. 2018; Čuk 2018; Smullen et al. 2016; Jackson et al. 2018), or by known or unknown planets (Bailer-Jones et al. 2018; Brassier & Morbidelli 2013; Charnoz & Morbidelli 2003; Correa-Otto & Calandra 2019; Duncan et al. 1987; Fernandez & Ip 1984; Portegies Zwart et al. 2018).

Bailer-Jones et al. (2018) produced an ejection speed distribution for the scattering of planetesimals by a giant planet orbiting a single star, and by a binary star with masses  $1 M_\odot$  and  $0.1 M_\odot$ . Though these parameters do not exactly match  $\alpha$  Cen’s, these models provide a reasonable first approximation to the speed distribution that we might expect for planetary and stellar ejections. We adopt the binary star speed distribution (the red dashed line in Fig. 6 of Bailer-Jones et al. (2018)) as being most applicable here, and it is shown in Figure 1. Note that it includes a low-velocity tail that covers the range of ejection speeds expected for planetary ejections as well, and indeed we will see in Section 3 that low-speed ejections are favored in terms of reaching our Solar System.

This ejection speed is taken as the asymptotic speed with which the particles leave  $\alpha$  Cen,  $v_\infty$ , and is multiplied by a directional vector (chosen randomly from the surface of a unit sphere) and added to the velocity of the star to determine the galactocentric velocity of the ejecta. The new ejected particle is placed within the simulation with the same position as the origin system and with this new velocity vector.

Between each time step of integration, the minimum distance between any particle and the Sun is interpolated by assuming a linear trajectory to avoid missing an encounter by stepping over it. If any particle passes within a specified

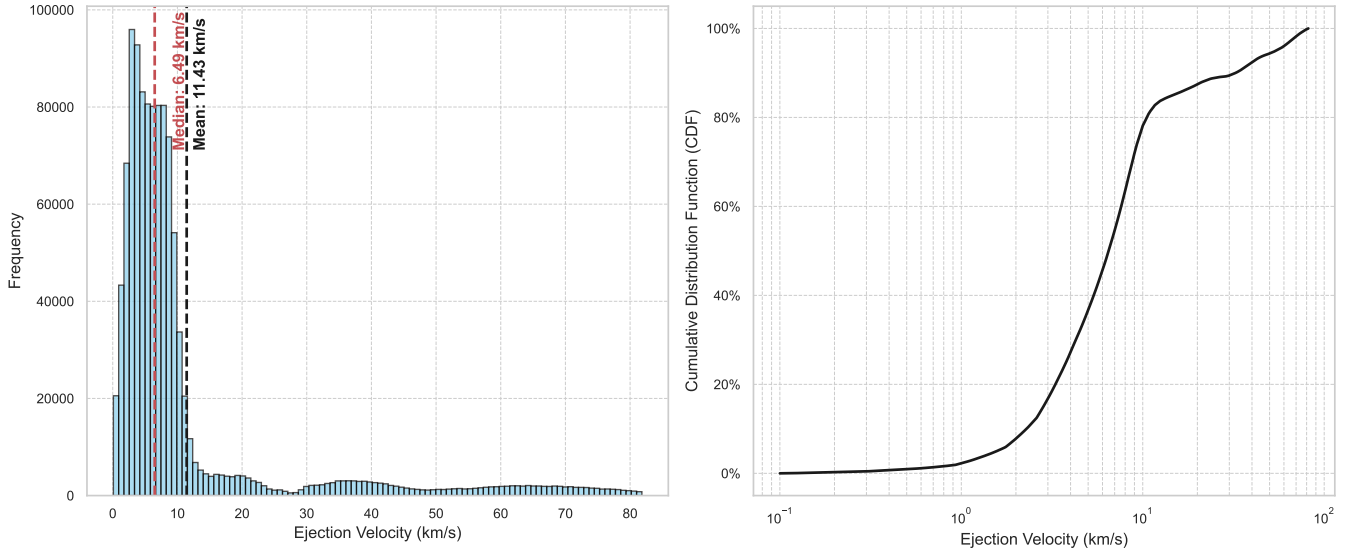


**Figure 1.** The ejection velocity distribution from our simulations, adapted from Figure 6 of [Bailer-Jones et al. \(2018\)](#) (their red-dashed line). The right panel is our recreation of the [Bailer-Jones et al. \(2018\)](#) figure, showing the cumulative distribution of ejection velocities caused from a binary star system with masses  $1 M_{\odot}$  and  $0.1 M_{\odot}$  on a circular orbit of with 10 au separation.

distance of the Sun (a heliocentric bubble of radius 100,000 au, chosen more or less arbitrarily but representative of the extent of the outer OC), the object is flagged as a close approach (CA), and all details are noted.

### 3. RESULTS

A total of  $1.09 \times 10^6$  particles were ejected from the  $\alpha$  Cen system throughout the simulation. As described in Section 2.2, the particles were ejected in random directions and their ejection speeds followed the distribution of [Bailer-Jones et al. \(2018\)](#). The simulation began at  $t \approx -100$  Myr and ended at  $t \approx 10$  Myr (Figure 2 and the corresponding animation).

Only a small fraction of the  $\alpha$  Cen ejecta come within the CA distance of the Sun. In total, 350 particles had a CA with the Solar System,  $\sim 0.03\%$  of the total ejecta. The first CA arrives at  $t \approx -2.85$  Myr. Material continues to arrive for  $\sim 10$  Myr (Figure 3 and the corresponding animation) with the majority of CAs within  $\pm 200,000$  yr of the current epoch (Figure 4). This peak is centered around  $\alpha$  Cen’s time of closest approach to the Solar System in  $\sim 28,000$  yr. In that figure we also include the effective cross-section of the Solar System (here taken to be of  $10^5$  au radius) as viewed from  $\alpha$  Cen and expressed as a solid angle. This cone reaches a maximum full-width of  $37.5^\circ$  when  $\alpha$  Cen is at its point of closest approach, and we see that the rate of arrivals broadly coincides with and peaks at the same time. However, because the particle travel times are not zero, this is only an approximation of the effective cross-section that they see and which depends on their relative velocity. Nevertheless, it illustrates that we expect material to be transferred more efficiently as our Solar System’s apparent cross-section grows as we move towards our point of closest approach with  $\alpha$  Cen.

The ejection speed distribution from a giant planet peaks between 1 and 2  $\text{km s}^{-1}$  ([Bailer-Jones et al. 2018](#)); while in our simulations we find 52% of particles that arrive from  $\alpha$  Cen have ejection speeds less than 2  $\text{km s}^{-1}$  (with a maximum around 77  $\text{km s}^{-1}$ , Figure 5). Thus, the speeds that most effectively move material from  $\alpha$  Cen to us closely match those expected for ejection by a massive planet, such as might occur due to the planets around Proxima Centauri, though no planets more massive than a mini-Neptune have yet been confirmed in the  $\alpha$  Cen system.

The times of ejection ( $t_{\text{eject}}$ ) that resulted in a CA ranged from  $t_{\text{eject}} \approx -93$  Myr to  $t_{\text{eject}} \approx -12,000$  yr. The majority of the CAs had ejection times closer to the current epoch ( $\approx 53\%$  with  $t_{\text{eject}} > -1$  Myr;  $\approx 84\%$  with  $t_{\text{eject}} > -10$  Myr), meaning that fresh ejecta was more likely to encounter the Solar System (Figure 5). This is as expected, as the  $\alpha$  Cen system is moving towards the Sun and the solid angle the Solar System subtends is largest when their mutual distance is smallest. The majority ( $\approx 84\%$ ) of the CAs traveled for  $< 10$  Myr, a fraction of a galactic orbit (Figure 6). These particles are therefore exposed to the ISM for a relatively short time, lessening any effects from

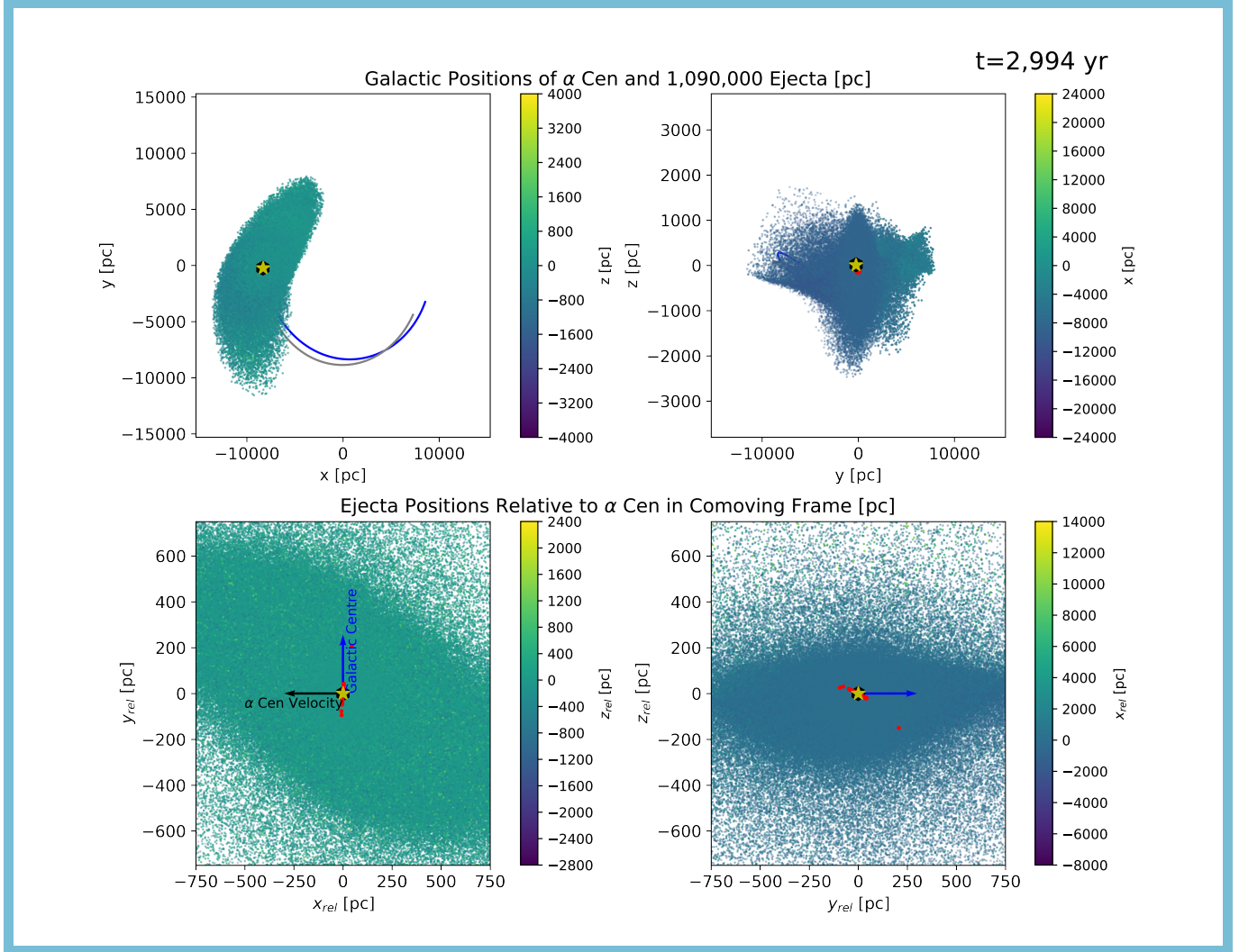


**Figure 2.**  $\alpha$  Cen's orbit about the Galactic Centre viewed on the xy and yz planes (top row), as well as the orbits of the ejecta from  $\alpha$  Cen viewed in a comoving frame (bottom row). Our Sun (*Sol*) is marked by a black hexagon and its orbital path indicated by a grey solid line (top row only).  $\alpha$  Cen's location and path are shown by a yellow star and blue solid line (top row only). In the bottom row, the comoving frame follows  $\alpha$  Cen around its orbit while maintaining its orientation with the y-axis pointing towards the Galactic Centre (blue arrow) and  $\alpha$  Cen's velocity pointing in the  $-x$  direction (black arrow). This still frame is taken at  $t \approx 3,000$  yr (that is, +3,000 years from the current epoch) after  $\sim 100$  Myr of integration. The colours of the ejecta represent the 3rd dimension of position, except that any particle that will at any point come within 100,000 au of *Sol* are plotted in red. The full animation is available in the HTML version of this publication which shows the time evolution from  $t \approx -100$  Myr to  $t \approx 10$  Myr. The duration of the animation is 11 s. <https://youtu.be/YABoYgNKr-I>

the galactic magnetic field, ISM drag, grain destruction, and perturbations from GMC encounters (discussed further in Section 4.1).

When the CAs intercept the Solar System, their median apparent velocity relative to the Sun ( $\Delta v$ ) observed at their closest approach is  $32.50 \text{ km s}^{-1}$ , ranging from  $13.75 \text{ km s}^{-1}$  to  $103.17 \text{ km s}^{-1}$  (Figure 7). Due to the high fraction of CAs that resulted from low ejection speeds, we see the solar relative velocities center around the current apparent velocity of  $\alpha$  Cen ( $\Delta v = 32.37 \text{ km s}^{-1}$ ) as expected.

As particles fall into the Solar System, their heliocentric speed  $v_{hel}$  increases beyond the relative speed  $\Delta v$  that they have at large distances. If they are observed on Earth as meteors, their observed heliocentric speed will be given by

$$v_{hel} = \sqrt{\Delta v^2 + \frac{2GM_{\odot}}{r_{\oplus}}} \quad (4)$$

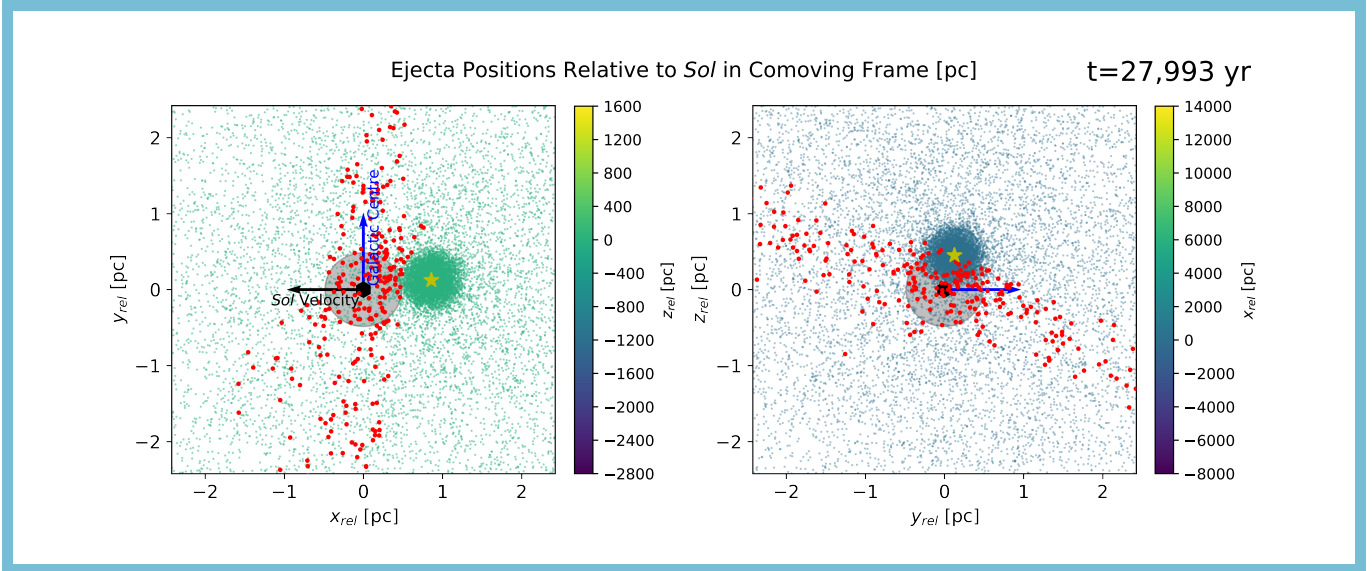


**Figure 3.** The paths of the ejecta from  $\alpha$  Cen viewed in a comoving frame with *Sol*. The comoving frame follows *Sol* around its orbit maintaining the orientation with the y-axis pointing towards the Galactic Centre (blue arrow) and *Sol*'s velocity pointing in the -x direction (black arrow). Our Sun (*Sol*) is indicated by a black hexagon and  $\alpha$  Cen by a yellow star. This still frame is taken at closest approach to our Solar System ( $t \approx 28,000$  yr, years from the current epoch) after  $\sim 100$  Myr of integration. The colours of the ejecta represent the 3rd dimension of position. The grey circle represents the extent of the Oort cloud (100,000 au), any particle that comes within this distance of *Sol* at any point is flagged as a close approach. These particles are plotted in red. The full animation is available in the HTML version of this publication which shows the shower duration from  $t \approx -3$  Myr to  $t \approx 7$  Myr. The duration of the animation is 44 s. <https://youtu.be/qxd5kguXRWw>

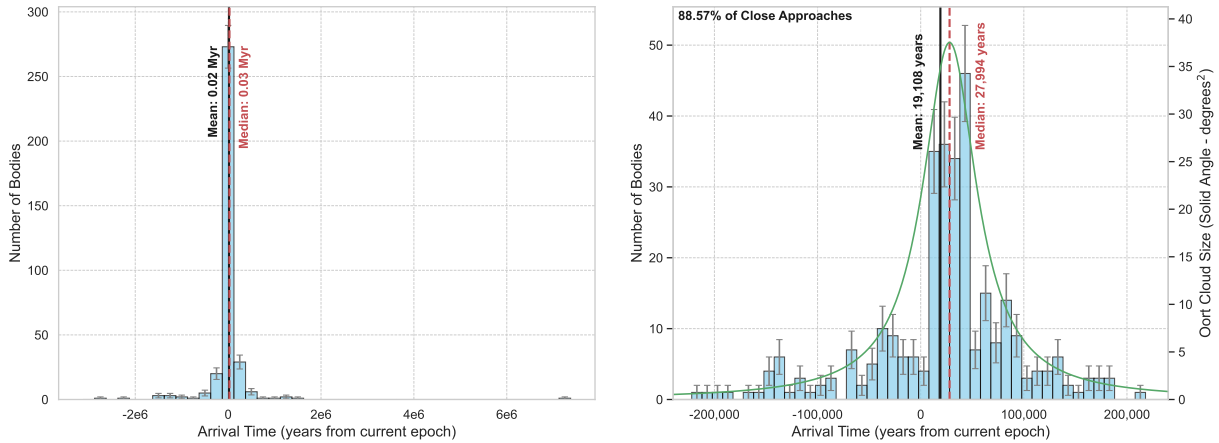


**Figure 4.** The arrival times at the Solar System of the  $\alpha$  Cen material. The left figure shows all close approaches while the right zooms into the time of peak intensity. The green line shows the effective cross-section of the Solar System (the solid angle subtended by our Oort cloud as seen from  $\alpha$  Cen).

where  $\Delta v$  is its velocity relative to the Sun when distant from our system and  $r_{\oplus}$  is the Earth's distance from the Sun. Using our minimum, median, and maximum values found, we can determine an expected range of heliocentric speeds in the inner Solar System, at 1 au from Sun, to be  $44 \lesssim v_{hel} \lesssim 111$  km s $^{-1}$  with a median around 53 km s $^{-1}$ .

### 3.1. Meteor Radiants

The heliocentric equatorial radiant of CAs is plotted in Figure 8, and also plotted and animated for the resulting “interstellar meteor shower” in Figure 9. The radiant would be the on-sky location from which the interstellar particle would appear to originate if it appeared as a meteor in Earth's sky. The figure converts the solar relative velocity

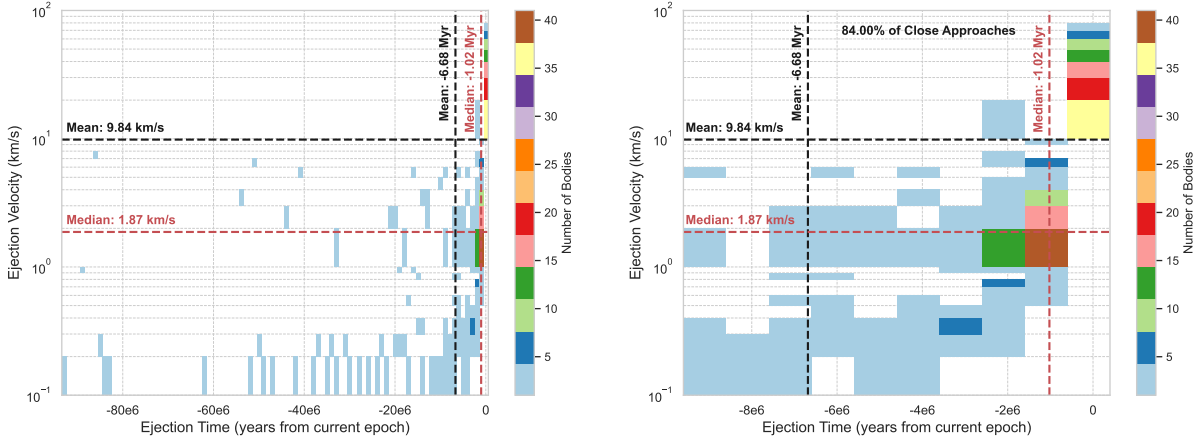


**Figure 5.** The ejection velocities vs time of ejection of the  $\alpha$  Cen material that enter our Oort cloud. The left figure shows the total distribution while the right zooms into the most common times.

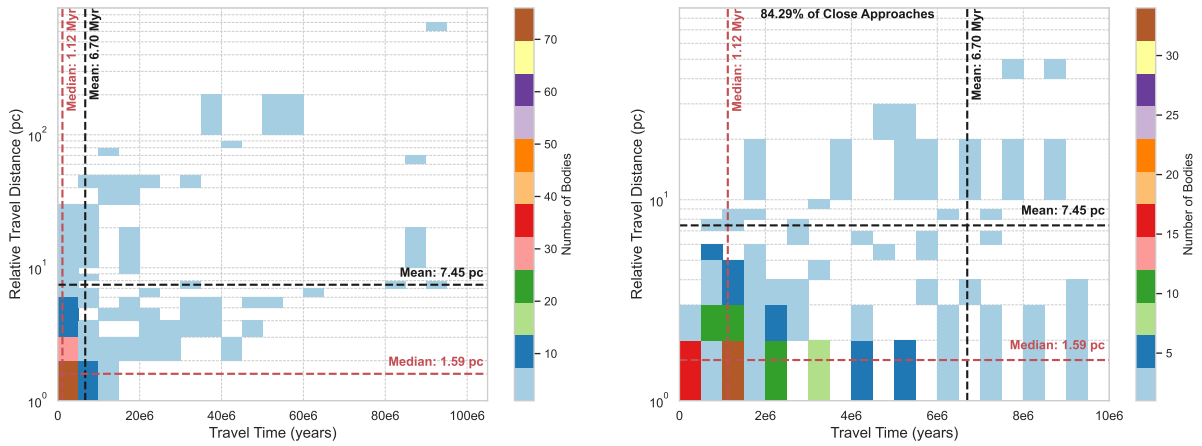


**Figure 6.** The relative travel distance (the distance a particle travels with respect to  $\alpha$  Cen) vs travel time of the  $\alpha$  Cen material that enter our Oort cloud. The left figure shows the total distribution while the right zooms into the most common times.

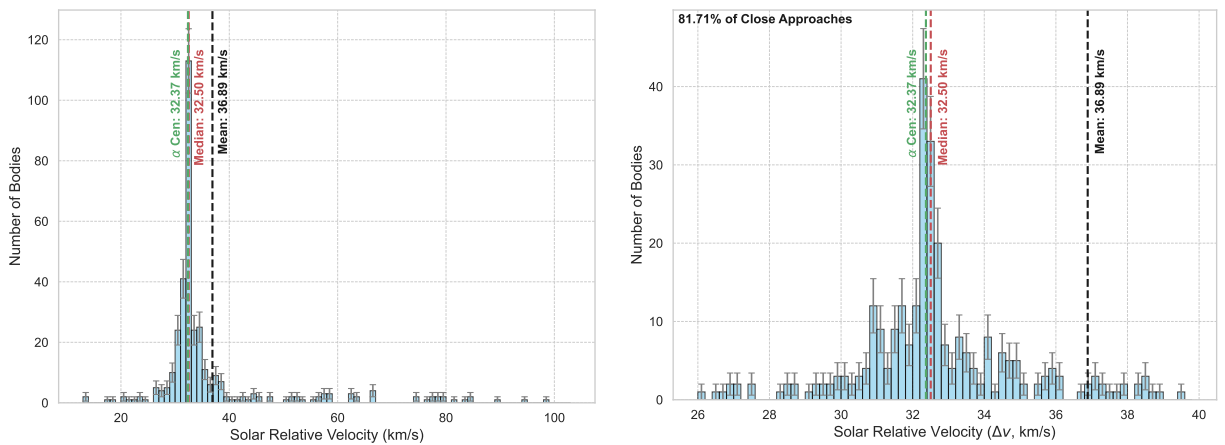


**Figure 7.** The apparent velocities of the  $\alpha$  Cen material that cross our Oort cloud. The left figure shows the total distribution while the right zooms into the most common speeds.

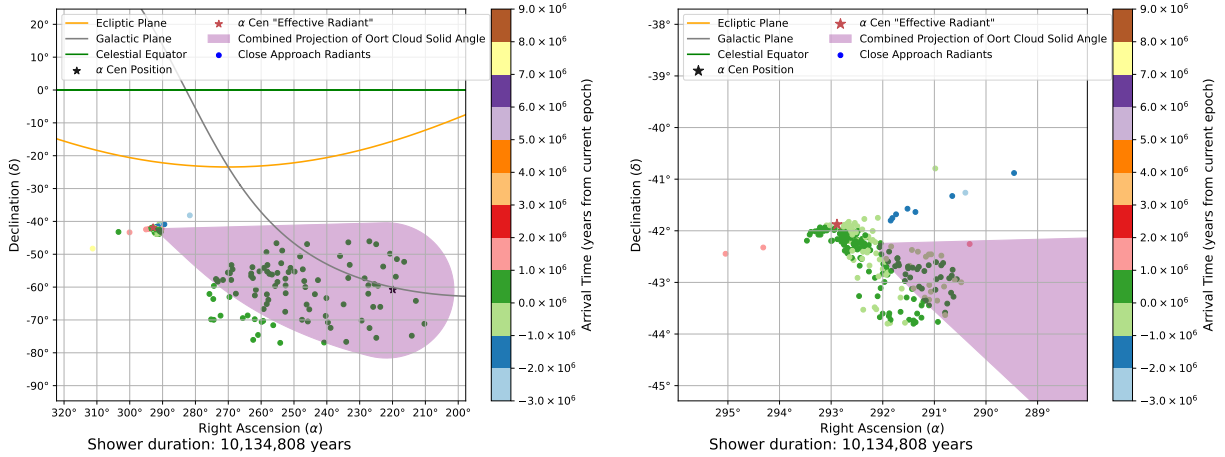


**Figure 8.** The heliocentric equatorial radiant for the 350 close approaches at the time of their closest Solar approach (“Arrival Time”), with the current heliocentric equatorial coordinates of  $\alpha Cen$  plotted as a black star and the “effective radiant” corresponding to  $\alpha Cen$ ’s apparent velocity is plotted as a red star. The purple shaded region is the combined projection of the the effective cross-section of the Solar System (solid angle size as seen from  $\alpha Cen$ ), from the start of the simulation up to the current time ( $t \approx 0$  yr). The left figure views the entire CA population while the right figure zooms into the region surrounding  $\alpha Cen$ ’s effective radiant.

( $\Delta v$ ) to a heliocentric equatorial right ascension (RA or  $\alpha$ ) and declination (Dec or  $\delta$ ) for easy comparison with Solar System meteor shower radiants. Two radiant clusters appeared in our simulations, one centered on an average position of  $(\alpha, \delta) = (292 \pm 1^\circ, -43 \pm 2^\circ)$  and the other at  $(\alpha, \delta) = (249 \pm 17^\circ, -60 \pm 8^\circ)$ .

The first cluster is located at the on-sky position of what we term the “effective radiant”, the projection of the  $\alpha Cen$ ’s velocity vector relative to the Sun (reversed) onto the celestial sphere. Currently  $\alpha Cen$ ’s motion relative to the Sun is one primarily of approach along the radial direction. Therefore particles originating from it and that arrive here must be traveling along that nearly same line, and thus the effective radiant coincides largely with  $\alpha Cen$ ’s position on the sky. One would expect the radiant of the stream to be in the approximate part of the sky as the origin star as it is approaching the Solar System. In the animation linked to Figure 9, we do indeed see the majority of the CAs coming from the same direction as both the on-sky position of  $\alpha Cen$  and its effective radiant, at least at times before the current epoch.

As  $\alpha Cen$  passes its closest point to us, its motion changes from being mostly radial to mostly tangential. Though particles continue to arrive in the Solar System from the direction of the effective radiant,  $\alpha Cen$  itself moves away from this point on the sky. The apparent cross-section of our Solar System is largest at closest approach, allowing material ejected with a range of speeds within a much wider cone to reach us, creating the broad second radiant cluster.

After  $\alpha Cen$  passes its closest approach, it begins to recede from us at  $32 \text{ km s}^{-1}$ ; however, low-speed material ejected in the past would still arrive from the same effective radiant. But at this point it is difficult for material newly ejected from that system to reach us, and the rate of arrival of material from  $\alpha Cen$  drops sharply.

The effective cross-section of the Solar System shows a smooth progression up to the peak intensity of the  $\alpha Cen$  shower (Figure 4). In our simulation, we instead see a more sudden increase, which result from our discrete ejection modeling. As we eject material every 1 Myr, we see a sudden burst of CAs around the time of  $\alpha Cen$ ’s closest approach, and a sudden shift in the radiant, rather than a gradual change. To examine this in more details, we ran an auxiliary simulation just during closest approach where the time between ejections was shortened. In this case, the CA radiants are smoothly dispersed along the path of the projected cross-section of the Solar System (purple shaded region in Figures 8 & 9) from a narrow cluster surrounding  $\alpha Cen$ ’s effective radiant to the large region near  $\alpha Cen$ ’s current on-sky position.

### 3.2. Are There $\alpha Cen$ Particles among proposed interstellars?

A selection of previously discovered/proposed interstellars are plotted along side the observed radiants of our  $\alpha Cen$  shower in Figure 9. Included are: two confirmed macroscopic interstellar objects (1I/Oumuamua and 2I/Borisov), traced back to their asymptotic arrival directions (Hallatt & Wiegert 2020); five unconfirmed interstellar meteoroid candidates observed by the Canadian Meteor Orbit Radar (CMOR) Froncisz et al. (2020)); three reported interstellar

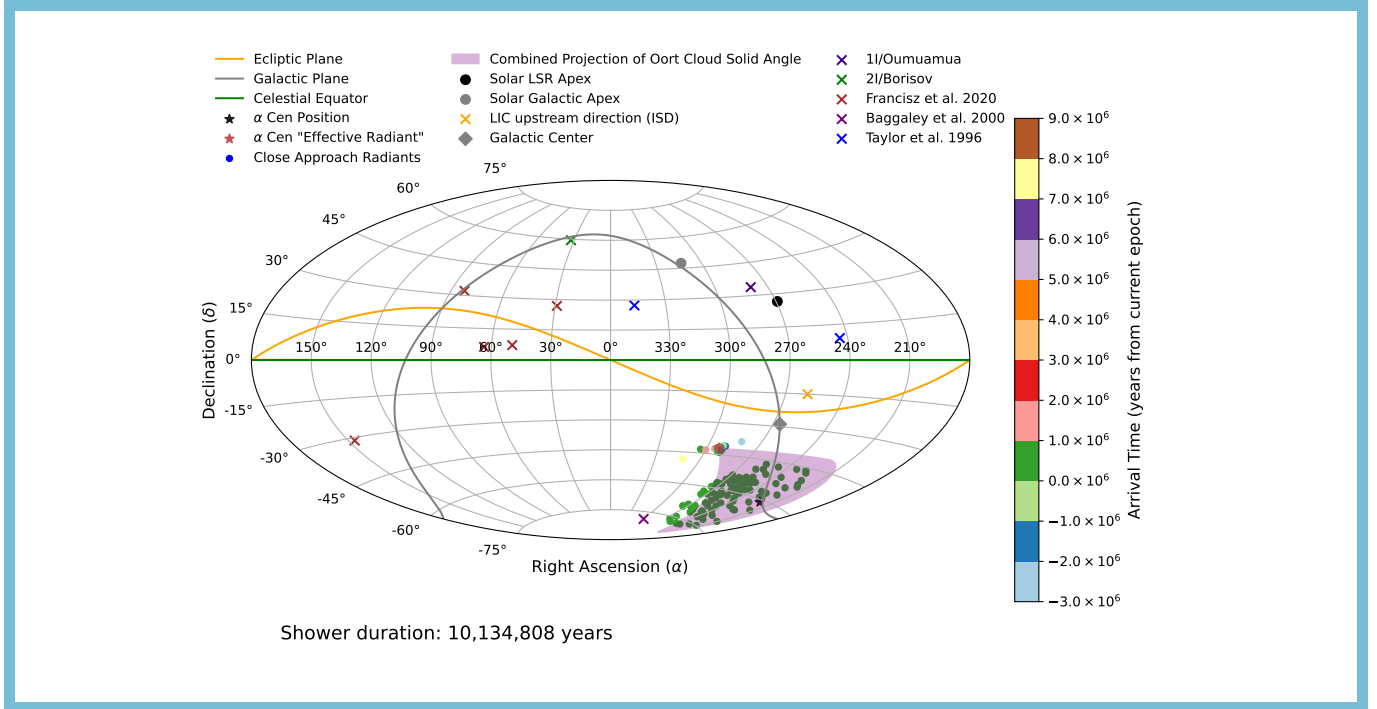


**Figure 9.** An all-sky version of Figure 8 (see that Figure for additional information), with the addition of the two confirmed km-scale interstellar objects (ISOs), 5 unconfirmed interstellar meteors, 3 suggested high interstellar meteor flux regions, and the direction of the local interstellar cloud (LIC) upstream direction of interstellar dust (ISD) for comparison (all summarized in Table 2). The Solar apex with respect to the Local Standard of Rest (LSR) and within the Milky Way are also included, along with the direction towards the Galactic Center. In the full HTML version of this publication an animation is available showing the radiant of the CAs as they appear during peak intensity, and the progression of  $\alpha$  Cen’s position and “effective radiant.” The duration of the animation is 41 s. <https://youtu.be/bu6849CAHkg>

meteor influx directions detected by the Advanced Meteor Orbit Radar (AMOR) (Baggaley 2000; Taylor et al. 1996); along with confirmed interstellar dust (ISD) influx directions into the Solar System as reported by spacecraft Cassini, Ulysses, and Galileo (Sterken et al. 2012). Other directions are also included for comparison, including the Solar apex with respect to the Local Standard of Rest (LSR) (Jaschek & Valbousquet 1992); the Solar apex with respect to the Galactic Center (Solar Galactic Apex) (Reid & Brunthaler 2004).

The list of values plotted in Figure 9 is provided in Table 2. None of these appears to be correlated with the directions expected for  $\alpha$  Cen. Further analysis of meteor databases to search for  $\alpha$  Cen-related events is encouraged.

## 4. DISCUSSION

Earlier sections have shown that there are plausible dynamical pathways from  $\alpha$  Cen to our Solar System. We now turn to a discussion of the particle sizes that can survive the passage from  $\alpha$  Cen to our Solar System, and the expected flux of such particles.

### 4.1. Grain sizes & Implications

Small particles traveling through the interstellar medium (ISM) are subject to a number of effects not modeled here. Thus, though in principle particles may travel between  $\alpha$  Cen and our Solar System, whether or not particles –in particular mm-sized and smaller particles that might be observed as meteors in Earth’s atmosphere– can survive the journey depends on various factors, such as travel time and speed relative to the ISM. Following Murray et al. (2004), we can compute the minimum particle size that can survive the journey from  $\alpha$  Cen to our Solar System. In particular, they examine three effects 1) whether the effect of magnetic fields on small charged grains will deflect them

**Table 2.** Reported interstellars, including LIC upstream direction and significant directional values in ICRS coordinates.

Designation	Right Ascension ( $\alpha$ ) (deg)	Declination ( $\delta$ ) (deg)	Category	References
1I/'Oumuamua	279.6	33.9	ISO	[3]
2I/Borisov	32.6	59.5	ISO	[3]
	29.1	26.8	meteor	[2]
	49.6	7.2	meteor	[2]
	63.7	6.2	meteor	[2]
	82.6	32.0	meteor	[2]
	146.6	-31.1	meteor	[2]
	299.0	-78.4	meteor flux	[1]
	244.0	9.2	meteor flux	[6]
	347.1	27.3	meteor flux	[6]
Local interstellar cloud (LIC) upstream direction	259	8	ISD	[5]
Solar apex relative to Local Standard of Rest (LSR)	258.7	-15.0		[4]
Solar Galactic Apex	313.3	47.5		This work
Galactic Centre (GC) - $(\lambda, b) = (0^\circ, 0^\circ)$	266.4	-28.9		[7]

**References**—[1] Baggaley (2000), [2] Froncisz et al. (2020), [3] Hallatt & Wiegert (2020), [4] Jaschek & Valbousquet (1992), [5] Sterken et al. (2012), [6] Taylor et al. (1996), [7] Reid & Brunthaler (2004)

significantly, 2) whether drag against the ISM will halt the grains and 3) whether the grain will be destroyed through sputtering by high-speed gas atoms or by grain-grain collisions.

We extracted the relevant parameters for each of the 350 CAs from our simulation and computed the minimum size needed for a grain traveling along that trajectory to survive all three effects (Murray et al. (2004)'s equations 44, 45, and 47 relating to drag force, gyroradius, and grain destruction, respectively). We find that minimum particle sizes ( $a$ , radius) of  $1.05 \leq a \leq 73.22 \mu\text{m}$ , with a median of  $3.30 \mu\text{m}$ , can survive their journey (using values:  $\rho = 3.5 \text{ g cm}^{-3}$ ;  $n_H = 1 \text{ cm}^{-3}$ ;  $U = 1 \text{ V}$ ,  $B = 5 \mu\text{G}$ ; and  $T_{gas} = 10^6 \text{ K}$ ). To clarify, our median particle size corresponds to a simulated particle that traveled 1.5 pc in  $\alpha \text{ Cen}$ 's comoving frame at an average velocity of  $16 \text{ km s}^{-1}$  with respect to the circular velocity of the Sun. At this size and speed, the particle can travel 125 pc in the ISM before grain destruction becomes relevant, 4200 pc for ISM drag, and only 1.5 pc for magnetic forces, and thus our typical particles are effectively magnetically limited. In fact, all of our particles are limited by magnetic forces.

At these small grain sizes, detectability by meteor radar instruments is limited. The practical lower limit to the size of meteoroids detected by currently operating meteor patrol radars like the Canadian Meteor Orbital Radar (CMOR, described further in the next section) is roughly  $100 \mu\text{m}$  in diameter. Particles at these sizes travel unimpeded for large distances across the Galaxy. For example, a  $100 \mu\text{m}$  particle travelling at our typical speed of  $17 \text{ km s}^{-1}$  could travel 369 pc before being substantially deflected by magnetic fields. Only 1 of our simulated particles traveled farther (600 pc), while the remaining 349 traveled  $< 200 \text{ pc}$  (Figure 6). We therefore adopt a fiducial meteor size of  $100 \mu\text{m}$  (diameter) at which the effects of drag, grain destruction and magnetic deflection do not present a concern in this context. But in any case, from this analysis we can conclude that our results are applicable from submillimeter particles up to large telescopically observable asteroids or comets.

We note an important size-independent effect that we ignore is the effect of encounters with GMCs, which can create  $\sim 10 \text{ km s}^{-1}$  kicks in velocity on objects orbiting with the Milky Way's disk, and which occur with a characteristic time of 200 Myr (Wielen 1977; Mihalas & Binney 1981). Our simulations here only extend for 100 Myr and most of the mass transfer observed occurs over much shorter time scales, so the effect of GMCs on our results is likely negligible.

#### 4.2. Mass/Number Influx Estimates

We can now begin to draw some conclusions on how many  $\alpha$  Cen particles we may expect to see in the Solar System currently and during the peak intensity of the shower. To do this, we must estimate the ejection rate for the  $\alpha$  Cen system.

Unfortunately, the rate of ejection of material from  $\alpha$  Cen is poorly constrained. As a first-order approximation, we assume that  $\alpha$  Cen ejects material at a rate similar to that of the Solar System at the current time. At macroscopic sizes, this includes ejection of asteroids recently escaped from the asteroid belt, as well as the ejection of comets arriving from the OC or stripped from it by the galactic tidal field. The best quantified of these processes is the ejection of new OC comets, and we will adopt it here as a proxy for our total ejection rate. Comets newly arriving in the inner Solar System from the OC are on nearly-unbound orbits, and planetary perturbations will scatter half onto more tightly bound orbits and eject the other half (Weissman 1979; Wiegert & Tremaine 1999). So, the rate at which OC comets are ejected in our Solar System is roughly half the arrival rate of new OC comets to the inner Solar System. The rates of long-period comet detection have been carefully studied. Boe et al. (2019) report a size-frequency distribution (SFD) of long-period comets, which are mostly new OC comets, based on observations from Pan-STARRS. During the 6.8 year survey in question, 229 comets were observed with a typical nucleus size of 4 km. Extending this to smaller but still telescopically accessible sizes using their observed size distribution, this corresponds to  $1.76 \times 10^3$  new OC objects of 100 m or greater diameter passing perihelion per year, or an ejection rate of  $\sim 0.5 \times 1.76 \times 10^3 = 9 \times 10^2$  objects  $> 100$  m per year. Therefore, if  $\alpha$  Cen ejects cometary material at a rate equal to our own Solar System, then  $9 \times 10^8$  comets are ejected per Myr. In our simulations,  $10^4$  particles are ejected every Myr, so a single simulated particle represents  $f_{sim} = 9 \times 10^8 / 10^4 = 9 \times 10^4$  real particles  $> 100$  m in diameter.

In our simulations, at the current time, approximately 5 particles are seen to enter the OC per 10,000 yr (Figure 4). Since each of our simulated particles corresponds to  $f_{sim}$  real objects larger than 100 m, this translates into a flux into the OC of  $5f_{sim}/10^4 = 45$  macroscopic particles per year.

Particles from  $\alpha$  Cen arrive with typical speeds of  $32 \text{ km s}^{-1}$  relative to the Sun and so take an average of  $\sim 20,000$  years to cross the 200,000 au diameter of the OC (assuming an average chord length of  $4R/3$ ). So an arrival flux of  $N$  per year into the OC translates into  $2 \times 10^4 N = 9 \times 10^5$  macroscopic particles from  $\alpha$  Cen currently within the OC. Although possibly abundant within the notional bounds of our Solar System, this number decreases significantly if we consider that our practical observation limit is only  $\leq 10$  au from the Sun. This region is only  $10^{-12}$  the volume of the OC and thus only expected to contain an object from  $\alpha$  Cen with probability  $\sim 10^{-6}$ .

Telescopically observable  $\alpha$  Cen interstellars are thus expected to be rare. But what about smaller particles, which are likely more abundant and could be observed by meteor monitoring systems? Determining the rate of ejection of particles at these sizes is even more difficult. We note here that Boe et al. (2019) SFD extends to  $\sim 120$  m: ideally, we would extend this to millimeter-sized particles, but the uncertainty in this process is too large to accurately make any sort of prediction on this basis.

Instead, for the sake of argument, let us consider the observability of an equivalent mass rate of ejection of  $100 \mu\text{m}$  particles, about the smallest meteor sizes routinely detected in Earth's atmosphere. This material could come from cometary material released from new  $\alpha$  Cen OC comets and then ejected by planetary perturbations much as the larger comets we considered above are, or could result from the breakup of ejected macroscopic comets in space. The question of mass ejection rates at these sizes surely deserves further study but is beyond the scope of this work.

Using our smallest comet size in this range (100 m) and an average comet density of  $400 \text{ kg m}^{-3}$  (A'Hearn et al. 2011; Sierks et al. 2015), an influx of 45  $\alpha$  Cen bodies 100 m in diameter translates to  $\sim 45 \times \frac{4\pi}{3} \times 50^3 \text{ m}^3 \times 400 \text{ kg m}^{-3} \approx 9.4 \times 10^9 \text{ kg}$  of  $\alpha$  Cen material per year. This same mass in  $100 \mu\text{m}$  diameter particles would provide  $10^{18}$  times more particles (or  $4.4 \times 10^{19}$ ). The relative cross-section of the Earth to that of the Oort cloud is  $\left(\frac{6378}{10^5 \times 1.5 \times 10^8} \text{ km}\right)^2 = 1.8 \times 10^{-19}$  and so we might expect  $(4.4 \times 10^{19}) \times (1.8 \times 10^{-19}) \approx 8$  meteors from  $\alpha$  Cen to enter the Earth's atmosphere per year as an upper limit. This number is very uncertain by any standard, but reveals that meteors from  $\alpha$  Cen may be currently detectable at Earth in small numbers.

During the peak intensity in  $\sim 28,000$  yr, we expect these values to increase by a factor of  $\sim 10$ : an influx of  $\sim 10^3$  macroscopic particles per year;  $10^7$  within the OC; a  $10^{-5}$  probability of one being within 10 au of the Sun; and  $10^2$  Earth intersecting  $100 \mu\text{m}$  particles per year.

To place this flux in context, we can compare it to the observed number of Solar System meteors that enter our atmosphere at these sizes. The Canadian Meteor Orbit Radar (CMOR) (Webster et al. 2004) is an all-sky meteor patrol radar that observes meteors above southwestern Ontario in Canada 24 hours a day down to a limiting mass of  $10^{-8} \text{ kg}$ , corresponding to  $200 \mu\text{m}$  (diameter) sizes for a density of  $1000 \text{ kg m}^{-3}$  ( $[574 \mu\text{m}, 135 \mu\text{m}]$  for densities of

[ $100 \text{ kg m}^{-3}$ ,  $7800 \text{ kg m}^{-3}$ ] corresponding to cometary material and iron respectively). CMOR observations provide the best measurements of meteor fluxes at sizes comparable to those we are considering here. [Froncisz et al. \(2020\)](#) provide the number of meteoroid orbits measured by CMOR and an integrated time-area product over 7.5 years of operation. From this, we can estimate that roughly  $7 \times 10^{12}$  meteoroids of all types (but essentially all from our Solar System) enter Earth’s atmosphere per year. As a result, only about 1 in  $10^{12}$   $100 \mu\text{m}$ -sized meteors observed at Earth might be from  $\alpha \text{ Cen}$ .

Meteors from  $\alpha$  Centauri are extremely rare events, vastly outnumbered by those originating in our Solar System. Nevertheless, understanding the properties of particles that could be arriving from  $\alpha \text{ Cen}$  will aid in the detection of these elusive but potentially highly informative visitors.

## 5. CONCLUSIONS

This work examines the possibility of material from our nearest stellar neighbour  $\alpha$  Centauri arriving at our Solar System. In particular we explored the delivery of sub-mm through km-sized bodies ejected from that system by gravitational scattering within the last 100 Myr.

Our study lead us to the following conclusions:

- Material from  $\alpha$  Centauri can reach and likely is already within our Solar System
- Most material arriving from  $\alpha$  Centauri has traveled for  $< 10$  Myr
- Material that reaches us typically left  $\alpha$  Centauri with low ( $v_\infty < 2 \text{ km s}^{-1}$ ) asymptotic speeds
- The delivery of particles from  $\alpha$  Centauri is concentrated during a  $\sim 10$  Myr period, with peak intensity centered after  $\alpha \text{ Cen}$ ’s closest approach ( $t \approx 28,000 \text{ yr}$ )
- The median velocity of the ejecta relative to the Sun at the time of close approach is  $\Delta v = 32.50 \text{ km s}^{-1}$ , similar to the current relative velocity of  $\alpha$  Centauri ( $\Delta v = 32.37 \text{ km s}^{-1}$  ([Wenger et al. 2000](#)))
- If any of this material enters the inner Solar System, its fall into the Sun’s gravitational well will accelerate it to a typical heliocentric velocity  $v_{hel} = 53 \text{ km s}^{-1}$  at 1 au
- The expected radiant of  $\alpha$  Centauri meteors at the current time ( $(\alpha, \delta) = (292^\circ \pm 1^\circ, -43^\circ \pm 2^\circ)$ ) largely corresponds to  $\alpha \text{ Cen}$ ’s effective radiant, set by that system’s velocity relative to the Sun. However, as  $\alpha \text{ Cen}$ ’s closest approach nears, the radiant will move and have a larger spread ( $(\alpha, \delta) = (249^\circ \pm 17^\circ, -61^\circ \pm 8^\circ)$ ) resulting from the increased range of allowable ejection speeds and directions near closest approach when the Solar System’s apparent cross-section is largest.
- We expect that particles larger than a few microns in size are able to survive the journey from  $\alpha$  Centauri
- If  $\alpha \text{ Cen}$  ejects comets at a rate comparable to the current Solar System rate, we expect  $\sim 10^6$  macroscopic  $\alpha$  Centauri particles to be currently within our Solar System, though the chance of one being detectable (that is, within 10 au of our star) is only one in a million.
- Estimates of  $\alpha$  Centauri meteor fluxes at the Earth are extremely uncertain, but a first approximation predicts perhaps as many as  $\sim 10$  detectable meteors per year in Earth’s atmosphere currently, and that the current rate should increase by a factor of 10 in the next 28,000 years

A thorough understanding of the mechanisms by which material could be transferred from  $\alpha$  Centauri to the Solar System not only deepens our knowledge of interstellar transport but also opens new pathways for exploring the interconnectedness of stellar systems and the potential for material exchange across the Galaxy.

This work was supported in part by the NASA Meteoroid Environment Office under Cooperative Agreement No. 80NSSC24M0060 and by the Natural Sciences and Engineering Research Council of Canada (NSERC) Discovery Grant program (grant No. RGPIN-2024-05200).

This research has made use of the SIMBAD database, operated at CDS, Strasbourg, France.

This work has made use of data from the European Space Agency (ESA) mission *Gaia* (<https://www.cosmos.esa.int/gaia>), processed by the *Gaia* Data Processing and Analysis Consortium (DPAC, <https://www.cosmos.esa.int/web/gaia/dpac/consortium>). Funding for the DPAC has been provided by national institutions, in particular the institutions participating in the *Gaia* Multilateral Agreement.

## REFERENCES

- Adams, F. C. 2010, Annual Review of Astronomy and Astrophysics, 48, 47, doi: [10.1146/annurev-astro-081309-130830](https://doi.org/10.1146/annurev-astro-081309-130830)
- Adams, F. C., & Napier, K. J. 2022, Astrobiology, 22, 1429, doi: [10.1089/ast.2021.0187](https://doi.org/10.1089/ast.2021.0187)
- Akeson, R., Beichman, C., Kervella, P., Fomalont, E., & Benedict, G. F. 2021, The Astronomical Journal, 162, 14, doi: [10.3847/1538-3881/abfaff](https://doi.org/10.3847/1538-3881/abfaff)
- Altbelli, N., Kempf, S., Landgraf, M., et al. 2003, Journal of Geophysical Research: Space Physics, 108
- Anglada-Escudé, G., Amado, P. J., Barnes, J., et al. 2016, Nature, 536, 437, doi: [10.1038/nature19106](https://doi.org/10.1038/nature19106)
- A'Hearn, M. F., Belton, M. J., Delamere, W. A., et al. 2011, Science, 332, 1396
- Baggaley, W. J. 2000, Journal of Geophysical Research: Space Physics, 105, 10353
- Baguhl, M., Grün, E., Hamilton, D., et al. 1995, The High Latitude Heliosphere, 471
- Bailer-Jones, C. A. L., Farnocchia, D., Meech, K. J., et al. 2018, The Astronomical Journal, 156, 205
- Binney, J., & Tremaine, S. 2008, Galactic Dynamics, 2nd edn. (Princeton, NJ: Princeton University Press)
- Boe, B., Jedicke, R., Meech, K. J., et al. 2019, Icarus, 333, 252, doi: <https://doi.org/10.1016/j.icarus.2019.05.034>
- Bovy, J. 2015, The Astrophysical Journal Supplement Series, 216, 29
- Brasser, R., & Morbidelli, A. 2013, Icarus, 225, 40
- Charnoz, S., & Morbidelli, A. 2003, Icarus, 166, 141
- Chen, B., Stoughton, C., Smith, J. A., et al. 2001, The Astrophysical Journal, 553, 184
- Correa-Otto, J. A., & Calandra, M. F. 2019, Monthly Notices of the Royal Astronomical Society, 490, 2495, doi: [10.1093/mnras/stz2671](https://doi.org/10.1093/mnras/stz2671)
- Cuello, N., & Sucerquia, M. 2024, Alpha Centauri: Disc Dynamics, Planet Stability, Detectability, arXiv. <http://arxiv.org/abs/2401.16003>
- Ćuk, M. 2018, The Astrophysical Journal Letters, 852, L15, doi: [10.3847/2041-8213/aaa3e2](https://doi.org/10.3847/2041-8213/aaa3e2)
- Damasso, M., Del Sordo, F., Anglada-Escudé, G., et al. 2020, Science Advances, 6, eaax7467, doi: [10.1126/sciadv.aax7467](https://doi.org/10.1126/sciadv.aax7467)
- Dauphole, B., & Colin, J. 1995, Astronomy and Astrophysics, 300, 117
- Dehnen, W., & Hasanuddin. 2018, Monthly Notices of the Royal Astronomical Society, 479, 4720, doi: [10.1093/mnras/sty1726](https://doi.org/10.1093/mnras/sty1726)
- Duncan, M., Quinn, T., & Tremaine, S. 1987, The Astronomical Journal, 94, 1330
- Evans, D. 1967, in Determination of Radial Velocities and their Applications, Vol. 30, 57
- Faria, J. P., Suárez Mascareño, A., Figueira, P., et al. 2022, Astronomy & Astrophysics, 658, A115, doi: [10.1051/0004-6361/202142337](https://doi.org/10.1051/0004-6361/202142337)
- Fehlberg, E. 1974, Classical seventh-, sixth-, and fifth-order Runge-Kutta-Nyström formulas with stepsize control for general second-order differential equations, Tech. rep., National Aeronautics and Space Administration
- Fernandez, J., & Ip, W.-H. 1984, Icarus, 58, 109
- Froncisz, M., Brown, P., & Weryk, R. J. 2020, Planetary and Space Science, 190, 104980
- Gillessen, S., Eisenhauer, F., Trippe, S., et al. 2009, The Astrophysical Journal, 692, 1075
- Gratton, R., Zurlo, A., Le Coroller, H., et al. 2020, Astronomy & Astrophysics, 638, A120, doi: [10.1051/0004-6361/202037594](https://doi.org/10.1051/0004-6361/202037594)
- Grishin, E., Perets, H. B., & Avni, Y. 2019, Monthly Notices of the Royal Astronomical Society, 487, 3324, doi: [10.1093/mnras/stz1505](https://doi.org/10.1093/mnras/stz1505)
- Grün, E., Staubach, P., Baguhl, M., et al. 1997, Icarus, 129, 270
- Guzik, P., Drahus, M., Rusek, K., et al. 2020, Nature Astronomy, 4, 53
- Hajdukova, M., Sterken, V., Wiegert, P., & Kornoš, L. 2020, Planetary and Space Science, 192, 105060, doi: [10.1016/j.pss.2020.105060](https://doi.org/10.1016/j.pss.2020.105060)

- Hajduková, M., Stober, G., Barghini, D., et al. 2024, *Astronomy & Astrophysics*, 691, A8, doi: [10.1051/0004-6361/202449569](https://doi.org/10.1051/0004-6361/202449569)
- Hallatt, T., & Wiegert, P. 2020, *The Astronomical Journal*, 159, 147
- Jackson, A. P., Tamayo, D., Hammond, N., Ali-Dib, M., & Rein, H. 2018, *Monthly Notices of the Royal Astronomical Society: Letters*, 478, L49
- Jaschek, C., & Valbousquet, A. 1992, *Astronomy and Astrophysics*, 255, 124. <https://ui.adsabs.harvard.edu/abs/1992A&A...255..124J>
- Joyce, M., & Chaboyer, B. 2018, *The Astrophysical Journal*, 864, 99, doi: [10.3847/1538-4357/aad464](https://doi.org/10.3847/1538-4357/aad464)
- Kervella, P., Thévenin, F., & Lovis, C. 2017, *Astronomy & Astrophysics*, 598, L7, doi: [10.1051/0004-6361/201629930](https://doi.org/10.1051/0004-6361/201629930)
- Meech, K. J., Weryk, R., Micheli, M., et al. 2017, *Nature*, 552, 378
- Mihalas, D., & Binney, J. 1981, *Galactic Astronomy* (New York: Freeman)
- Miyamoto, M., & Nagai, R. 1975, *Publications of the Astronomical Society of Japan*, 27, 533
- Morel, P., Provost, J., Lebreton, Y., Thevenin, F., & Berthomieu, G. 2000, *Calibrations of alpha Cen A & B*, arXiv, doi: [10.48550/arXiv.astro-ph/0010180](https://doi.org/10.48550/arXiv.astro-ph/0010180)
- Moro-Martín, A., & Norman, C. 2022, *The Astrophysical Journal*, 924, 96
- Murray, N., Weingartner, J. C., & Capobianco, C. 2004, *The Astrophysical Journal*, 600, 804
- Osmanov, Z. N. 2024, *The possibility of panspermia in the deep cosmos by means of the planetary dust grains*, arXiv. <http://arxiv.org/abs/2402.04990>
- Portegies Zwart, S. 2021, *Astronomy and Astrophysics*, 647, doi: [10.1051/0004-6361/202038888](https://doi.org/10.1051/0004-6361/202038888)
- Portegies Zwart, S., Torres, S., Pelupessy, I., Bédorf, J., & Cai, M. X. 2018, *Monthly Notices of the Royal Astronomical Society: Letters*, 479, L17, doi: [10.1093/mnrasl/sly088](https://doi.org/10.1093/mnrasl/sly088)
- Rajpaul, V., Aigrain, S., & Roberts, S. J. 2015, *Monthly Notices of the Royal Astronomical Society: Letters*, 456, L6, doi: [10.1093/mnrasl/slv164](https://doi.org/10.1093/mnrasl/slv164)
- Reid, M. J., & Brunthaler, A. 2004, *The Astrophysical Journal*, 616, 872
- Ribas, I., Gregg, M. D., Boyajian, T. S., & Bolmont, E. 2017, *Astronomy & Astrophysics*, 603, A58, doi: [10.1051/0004-6361/201730582](https://doi.org/10.1051/0004-6361/201730582)
- Safronov, V. S. 1972, in *The Motion, Evolution of Orbits, and Origin of Comets*, ed. G. A. Chebotarev, E. I. Kazimirchak-Polonskaya, & B. G. Marsden (New York: Springer), 329–334
- Schönrich, R., Binney, J., & Dehnen, W. 2010, *Monthly Notices of the Royal Astronomical Society*, 403, 1829
- Sierks, H., Barbieri, C., Lamy, P. L., et al. 2015, *Science*, 347, aaa1044
- Smith, H. B., & Sinapayen, L. 2024, *An Agnostic Biosignature Based on Modeling Panspermia and Terraformation*, arXiv. <http://arxiv.org/abs/2403.14195>
- Smullen, R. A., Kratter, K. M., & Shannon, A. 2016, *Monthly Notices of the Royal Astronomical Society*, 461, 1288, doi: [10.1093/mnras/stw1347](https://doi.org/10.1093/mnras/stw1347)
- Sterken, V. J., Altobelli, N., Kempf, S., et al. 2012, *Astronomy & Astrophysics*, 538, A102, doi: [10.1051/0004-6361/201117119](https://doi.org/10.1051/0004-6361/201117119)
- Taylor, A. D., Baggaley, W. J., & Steel, D. I. 1996, *Nature*, 380, 323, doi: [10.1038/380323a0](https://doi.org/10.1038/380323a0)
- Thévenin, F., Provost, J., Morel, P., et al. 2002, *Astronomy & Astrophysics*, 392, L9, doi: [10.1051/0004-6361:20021074](https://doi.org/10.1051/0004-6361:20021074)
- Torres, S., Cai, M. X., Brown, A. G. A., & Zwart, S. P. 2019, *Astronomy & Astrophysics*, 629, A139, doi: [10.1051/0004-6361/201935330](https://doi.org/10.1051/0004-6361/201935330)
- Tremaine, S. 1993, in *Astron. Soc. Pac. Conference Series*, Vol. 36, *Planets around Pulsars*, ed. J. A. Phillips, S. E. Thorsett, & S. R. Kulkarni (San Francisco: Astronomical Society of the Pacific), 335–344
- Wagner, K., Boehle, A., Pathak, P., et al. 2021, *Nature Communications*, 12, 922, doi: [10.1038/s41467-021-21176-6](https://doi.org/10.1038/s41467-021-21176-6)
- Webster, A., Brown, P., Jones, J., Ellis, K., & Campbell-Brown, M. 2004, *Atmospheric Chemistry and Physics*, 4, 679
- Weissman, P. R. 1979, in *Dynamics of the Solar System*, ed. R. L. Duncombe (Boston: D. Reidel), 277–282
- Wenger, M., Ochsenein, F., Egret, D., et al. 2000, *A&AS*, 143, 9, doi: [10.1051/aas:2000332](https://doi.org/10.1051/aas:2000332)
- Wiegert, P., & Tremaine, S. 1999, *icarus*, 137, 84
- Wielen, R. 1977, *Astronomy and Astrophysics*, 60, 263